ELASTIC AND PLASTIC INTERLAMINAR SHEAR DEFORMATION IN LAMINATED COMPOSITES UNDER GENERALIZED PLANE STRESS*

A. Levy†
H. Armen, Jr.†
J. Whiteside‡

Grumman Aerospace Corporation
Bethpage, New York 11714

Elastic and plastic interlaminar shear deformation in a laminated fibrous composite is studied by means of a finite-element method. A composite element, constructed of orthotropic membranes separated by shear-resisting media, is developed and utilized. The effect of interlaminar shear deformation at the free edges of solid laminates and laminates containing a cutout is presented.

I. INTRODUCTION

Interlaminar shear deformation, the mechanism by which load is transferred through a matrix material between two stiff laminae as the laminae tend to slide over each other, cannot be predicted by using classical plate theory. This type of deformation develops along the edges of a laminate and can be important with respect to strength predictions of composite structures, especially for a laminate with a relatively low transverse shear strength. Analogous behavior is found to exist in bonded structural joints.

Recognition of this phenomenon has generated interest in the development of analytic methods that can account for interlaminar shear deformation. Recently, this type of deformation has been described from three different viewpoints (Refs. 1-3) for the elastic behavior of a rectangular laminate. In Ref. 1 an exact

---

*These results were obtained in the course of work sponsored by the Air Force Flight Dynamics Laboratory under Contract F33615-70-C-1308.

†Research Scientist

‡Structural Mechanics Engineer

solution is presented for a model in which the fiber-bearing layers are replaced by homogeneous membranes with orthotropic properties and are separated by layers that develop only interlaminar shearing stresses. In Ref. 2, the exact equations of elasticity are solved by using a finite difference method. Here each lamina is assumed to be homogeneous, so that there is no physical separation of fibers and matrix through the thickness. Both solutions are applicable for the analysis of a finite laminate in regions removed from the loaded ends. In Ref. 3, a finite-element method is employed, using a model similar to that of Ref. 1, to analyze a rectangular panel of $\pm 45°$ angle ply construction.

In this paper, a finite-element method is employed to investigate the interlaminar shear behavior along straight boundaries and around circular cutouts in balanced laminates. The laminates are balanced in the sense that the laminae are symmetrically placed about the midplane so that no warping exists, that is, there is no bending generated as a result of stretching. From the previous studies (Refs. 1-3), there is sufficient evidence to indicate that the interlaminar shear stress may be of sufficient magnitude to cause plastic deformation of the matrix material. Therefore, a method to account for the effects of plasticity is included in the analysis. In addition, consideration is given to cyclic loading conditions involving reversed plastic deformation. This study is limited in that it provides for interlaminar plastic deformation only, i.e., the elements representing the in-plane behavior are assumed to remain elastic throughout the entire load history, while those elements representing the interlaminar shear behavior can assume elastic-plastic properties. While this does not provide a complete description of the coupled situation resulting from both types of plastic deformation, it does enable us to isolate the effect of interlaminar plastic deformation.

A brief description of the element and formulation of the governing matrix equation is followed by results for rectangular laminates in both the elastic and inelastic ranges. These results, obtained for solid laminates and laminates containing a circular cutout, show the effect of interlaminar shear deformation at free edges.

II. THE COMPOSITE ELEMENT

The idealized model separates the membrane and interlaminar properties of a laminated composite by using alternating orthotropic fiber-bearing segments and isotropic shear segments, as

shown in Fig. 1. The orthotropic segments carry in-plane stresses only, and may be considered to be in a state of plane stress; the shear segments carry only interlaminar shear stresses, and are in a state of pure shear. This is the same model as that used in Refs. 1 and 3.

The composite element consistent with the idealized model is shown in Fig. 2. The membrane segments are triangular orthotropic elements in which the total strains are assumed to be uniform (Ref. 4). Here the strain-displacement relation is based on a linearly varying displacement field. The stiffness properties of the interlaminar shear segments are also based on a linear displacement field, so that the shear strains may be written in terms of the nodal displacements in the following manner:

$$\gamma_{xz} = \frac{\partial u}{\partial z} = \left(u_i^{\ell-1} + u_j^{\ell-1} + u_k^{\ell-1} - u_i^{\ell} - u_j^{\ell} - u_k^{\ell}\right) / 3t$$

$$\gamma_{yz} = \frac{\partial v}{\partial z} = \left(v_i^{\ell-1} + v_j^{\ell-1} + v_k^{\ell-1} - v_i^{\ell} - v_j^{\ell} - v_k^{\ell}\right) / 3t \quad ,$$

where u and v are displacements in the x and y directions, respectively, subscripts identify element vertices, and superscripts identify element faces as shown in Fig. 2. Since the displacements vary linearly in the plane of a membrane segment, the interlaminar shear strain is computed on the basis of centroidal values of displacement, and thus the shear segment may be regarded as a shear-resisting medium connecting the centroids of adjacent membrane segments. Any number of segments may be stacked through the thickness to form the multilayered composite element.

III. FORMULATION OF GOVERNING MATRIX EQUATION

The formulation of the governing matrix equation is developed within the framework of the displacement method of finite-element analysis and follows that method as presented in Ref. 5. Accordingly, assumptions concerning the displacement field within an individual element are made in terms of discrete quantities at node points. In addition, independent assumptions may be made concerning the distribution of initial strain within an element. These assumptions concerning displacements and initial strains are used to derive the force-displacement relations for an individual element. This is accomplished by application of the principle of

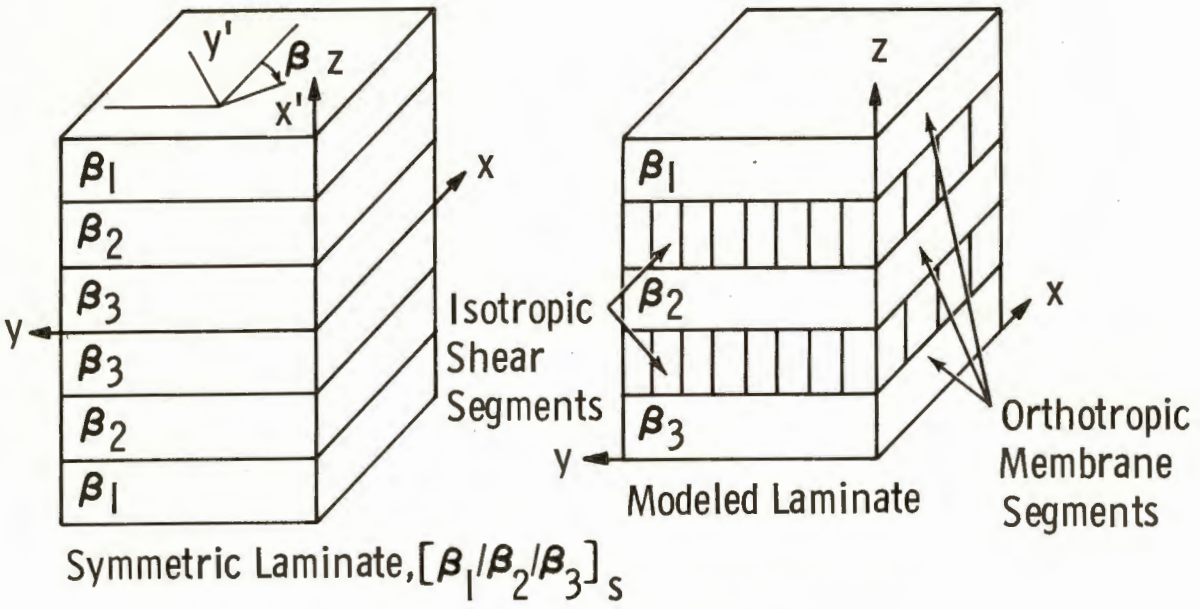

Figure 1. Laminate Model

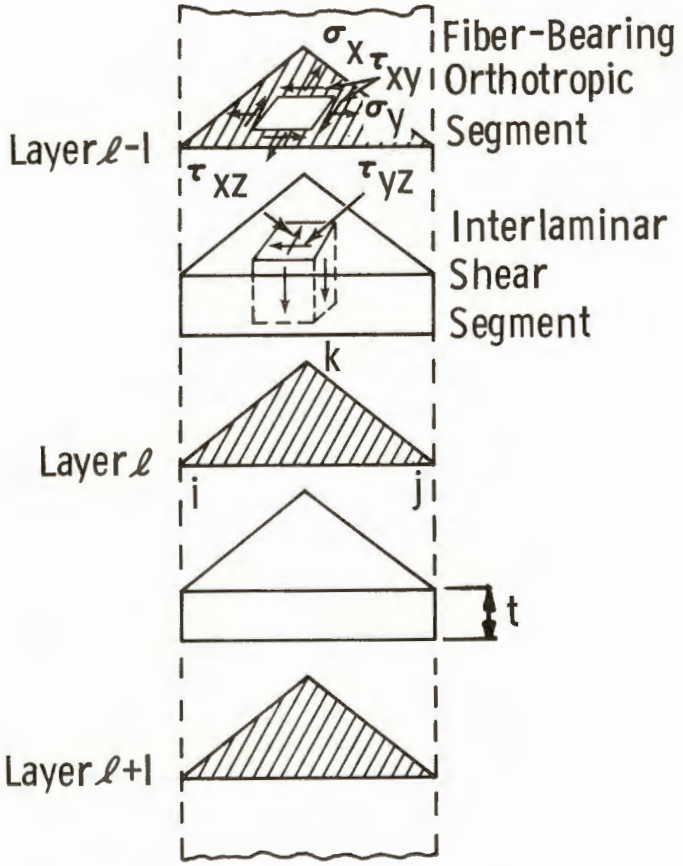

Figure 2. Composite Element

virtual work or through a consistent energy approach. The technique used to incorporate the effects of plastic behavior into a finite-element analysis is based on the initial strain concept (Ref. 5), according to which plastic strains (interlaminar shear components only) are interpreted as initial strains. At any step of the loading process, this procedure leads to the following governing linear matrix equation, in which generalized displacements, $\underset{\sim}{u}$, are related to applied loads $\underset{\sim}{f}$ and to the plastic shear strains, $\underset{\sim}{\gamma}_p$,

$$\underset{\sim}{f}^i = \underset{\sim}{k}\,\underset{\sim}{u}^i - \underset{\sim}{k}_p\underset{\sim}{\gamma}_p^i \tag{1}$$

where the superscript i refers to the current load step and where $\underset{\sim}{k}$ and $\underset{\sim}{k}_p$ represent the element stiffness and initial strain stiffness matrices, respectively. These element matrices are defined in Appendix A for a linear displacement field element in which the components of both total and plastic strains are uniform throughout.

If, in Eq. (1) the product of the initial strain stiffness matrix and the vector of plastic shear strains are considered as a vector of "effective plastic load," the equation may be rewritten by grouping together the generalized applied nodal forces and effective plastic loads, resulting in the following equation,

$$\underset{\sim}{f}^i + \underset{\sim}{q}^i = \underset{\sim}{k}\,\underset{\sim}{u}^i \tag{2}$$

where

$$\underset{\sim}{q}^i = \underset{\sim}{k}_p\underset{\sim}{\gamma}_p^i \quad .$$

A solution for the displacement $\underset{\sim}{u}^i$ in Eq. (2) requires that the value of the effective plastic load be known at the current load level, or alternatively be expressed in terms of $\underset{\sim}{u}^i$. Since the values of the plastic shear strain are not known at the current load step, and since they cannot be conveniently expressed in terms of the generalized nodal displacements, we employ a predictor procedure solution technique in which the effective plastic loads are based on values of plastic strains determined in the preceding load step. Consequently, Eq. (2) is written in the following form:

$$\underset{\sim}{f}^i + \underset{\sim}{q}^{i-1} = \underset{\sim}{k}\,\underset{\sim}{u}^i \tag{3}$$

where

$$\underset{\sim}{q}^{i-1} = \underset{\sim}{k}_p \underset{\sim}{\gamma}_p^{i-1}$$

and the superscript i-1 refers to the previous load level.

The use of this type of predictor procedure results in a "drifting" of the results from an exact solution as the loading increases. However, the inaccuracies can be minimized by using small load increments. The resulting accuracy and computing times required for this procedure were found to be competitive with those that utilize an iterative procedure and/or those in which plastic stress-strain relations are introduced explicitly into the governing matrix equations, thereby requiring a reformulation of the element stiffness matrices for each increment (i.e., tangent modulus method). These conclusions are based on experiences encompassing a wide variety of problems (Refs. 5 and 6), not exclusively associated with the particular class of problems treated here. A more detailed discussion of convergence and efficiencies associated with iterative methods of plastic analysis is presented in Ref. 7.

Equation (3) is written for each element in the structural idealization, and then, by an appropriate process of assemblage, the over-all linear matrix equation for the entire structure is formed. This resulting equation is identical in form to that of Eq. (3). Thus, with the present technique, one converts the nonlinear problem into a sequence of linear problems. Material nonlinearity is accounted for by introducing subsidiary incremental stress-strain relations from an appropriate plasticity theory and by the subsequent modification of applied loading through the effective plastic load. For the results presented here, the constitutive relations in the plastic range are developed on the basis of Drucker's postulate for work-hardening materials and the Prager-Ziegler kinematic hardening theory (Refs. 8 and 9), which accounts for the Bauschinger effect in the case of reversed plastic deformation. Details associated with the implementation of kinematic hardening in the finite-element analysis are presented in Refs. 5 and 6.

IV. ELASTIC RESULTS

Rectangular Panel

A flat rectangular panel is loaded axially along two opposite edges, which are assumed to remain straight and parallel but free to strain along their length. Since we are considering layups symmetrically placed about the midplane, no interlaminar shear stresses develop in the middle surface, and we may consider only that part of the panel on one side of the middle surface. As a result of symmetric geometry and loading conditions, a rotation of 180 degrees about the z-axis results in identical stress and deformation patterns. Therefore only one quarter of the panel, as shown by the shaded area in Fig. 3, need be considered for analysis. Furthermore, for layups in which a rotation of 180 degrees of the structure on one side of the midplane about the x-axis results in identical stress and deformation patterns, viz., a $[\beta_1/\beta_2/.../-\beta_2/-\beta_1]_s$ laminate, only one-eighth of the panel need be considered. The idealization used for such a case is shown in Fig. 4.

Results for a four ply $[\pm 45]_s$ angle ply laminate of boron-epoxy construction are shown in Fig. 5. The results compare favorably with the solution of Ref. 1. The interlaminar region in which the stress fields diverge from the classical plate solution comprises a narrow region along the free edge of the laminate and its "width of influence" is approximately 1.25 laminate thicknesses (5 lamina thicknesses). This interlaminar region, being one of high stress gradient, is sensitive to the ratio t/c, the ratio of a lamina thickness to a linear in-plane dimension of an element. For a structure in which the stresses along one edge, $y = b$, are not influenced by the free edge $y = -b$, the stress field is independent of the width. For problems involving widths greater than this limiting value, the same idealization can be used to determine the effect of various values of t/c by varying the thickness, t. Figure 6 shows some typical results in which good agreement with the exact solution is obtained for values of $t/c \geq 0.4$. Values of $t/c > 1/3$, or $t/\bar{c} > 1$ may be used as a guide to the construction of a finite-element idealization, where $\bar{c}$ is the distance from the centroid of the element to the free edge. Elements whose centroidal distance from an edge are greater than one lamina thickness (1/5 "width of influence") will not in general accurately predict the interlaminar effect.

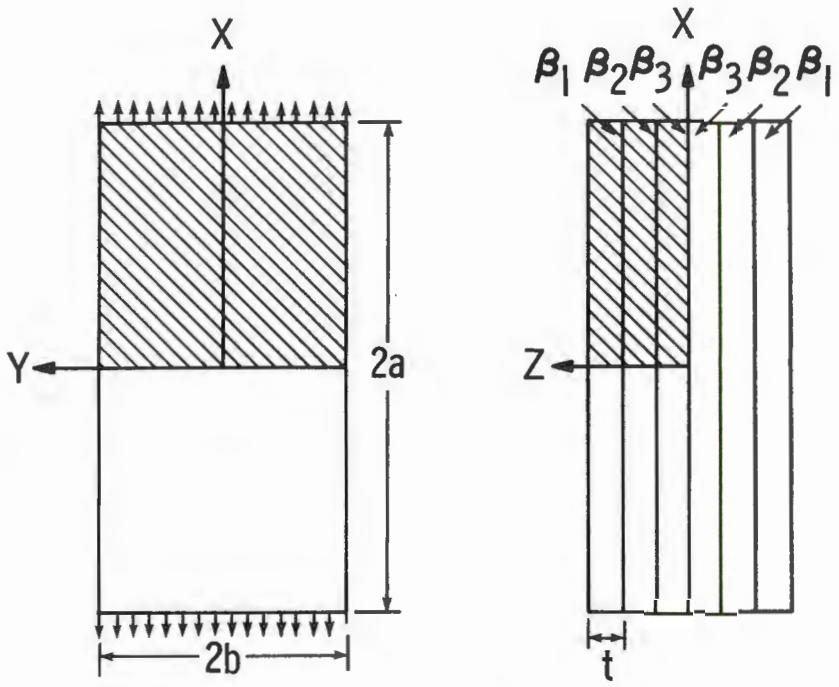

Figure 3. Laminate Geometry

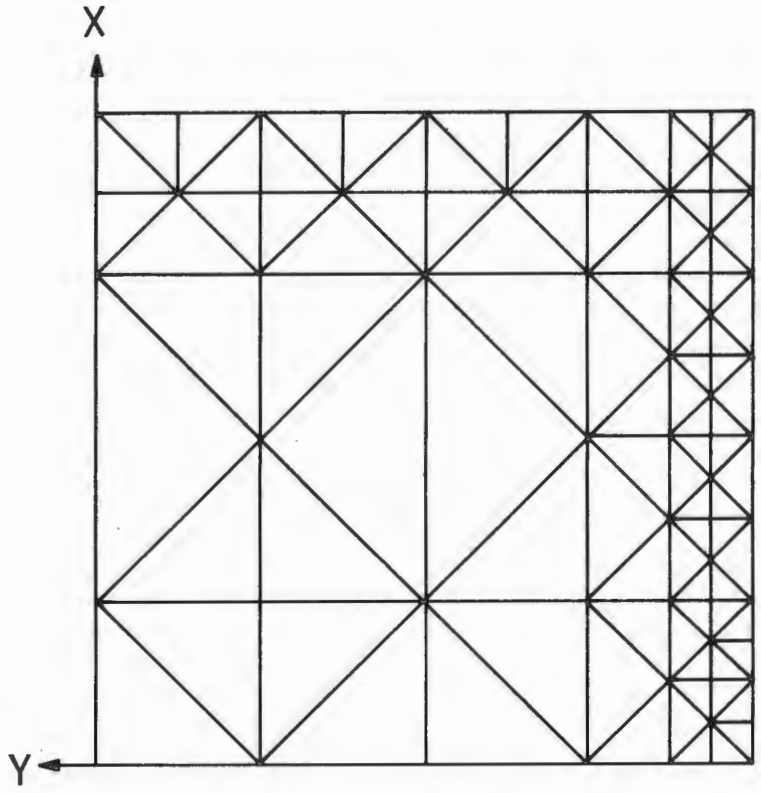

Figure. 4. Idealization of Quarter Panel

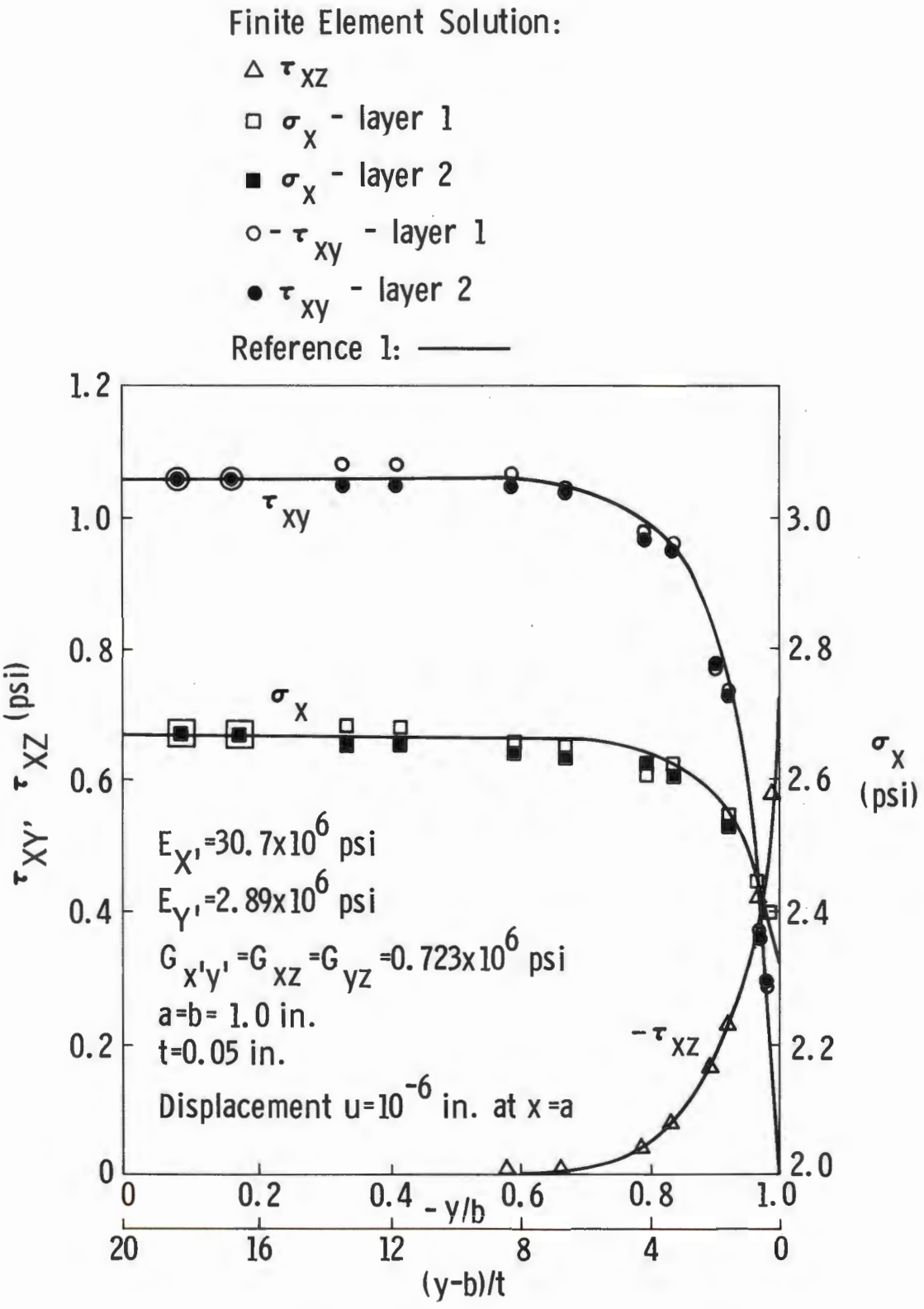

Figure 5. Stress Distributions, $[\pm 45]_s$ Laminate

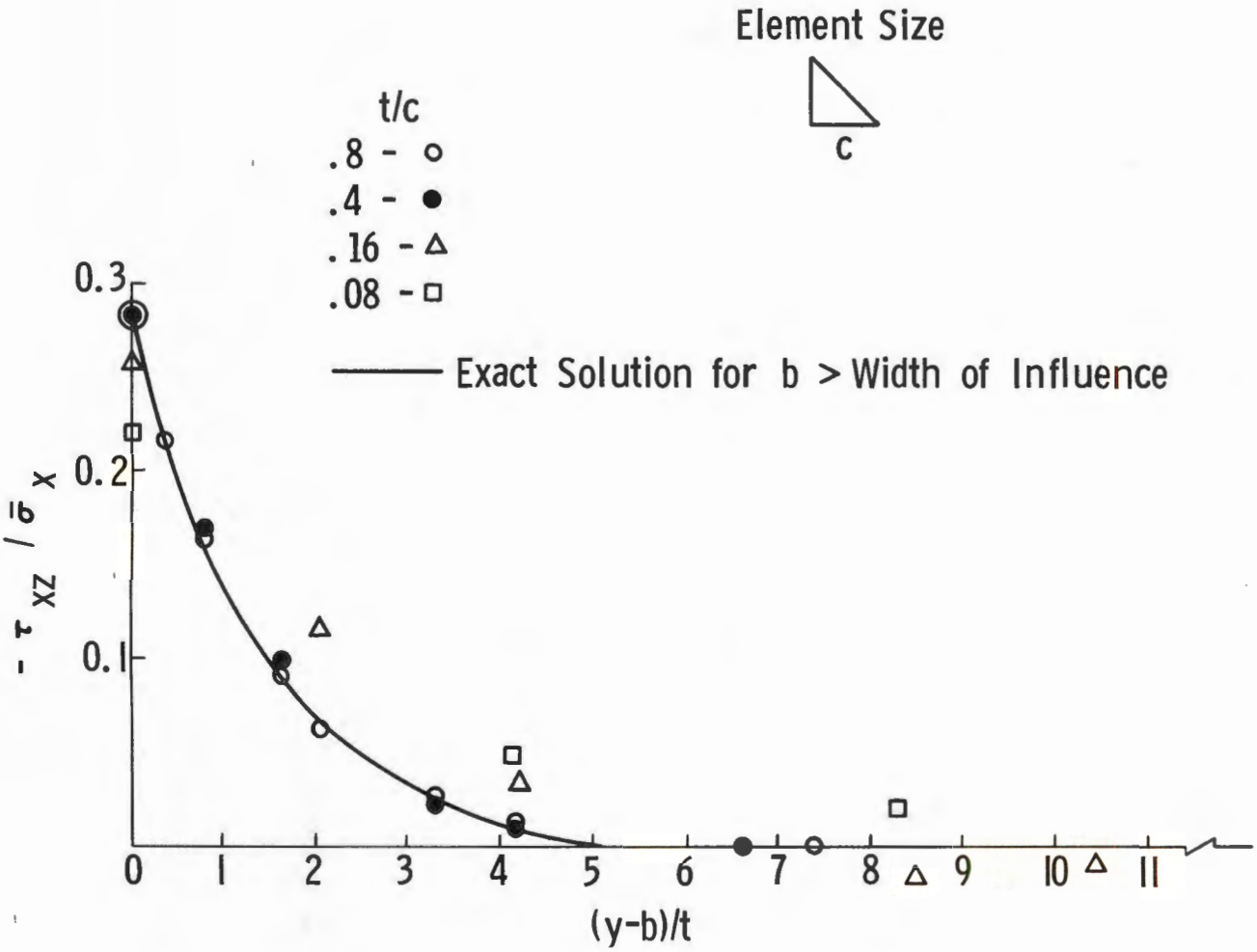

Figure 6. Computed Interlaminar Shear Stress Distribution for Various Ratios of t/c, $[\pm 45]_s$ Laminate.

The influence of a particular construction of a finite-element idealization on the results for membrane stresses in a two dimensional problem is discussed in Ref. 10 where it is shown that deviations of stress from the true solution are caused by inaccuracies in the shear stiffness resulting from the use of certain types of finite-element patterns. The idealization shown in Fig. 4 has mixed patterns that should cause a fluctuation about the true solution rather than a consistent underprediction or overprediction of stresses. This is substantiated by an inspection of Fig. 5. From these results, however, the in-plane idealization does not appear to influence the interlaminar shear stress.

Different results are obtained when modeling a lamina as homogeneous, as in Ref. 2, as compared with the present model in which the fiber-bearing region and matrix region are considered distinct through the thickness. Using the present techniques, one can investigate an entire spectrum of models ranging from a discrete to a homogeneous one. This is done by dividing each lamina into a number of segments through the thickness, representing fiber-bearing and matrix regions alternately. As the number of segments increases, the individual laminae approach homogeneity. This is illustrated by the results shown in Fig. 7, where each layer is idealized into one, two, and three membrane segments, separated by shear segments, and compared with the results of Ref. 2 for a graphite-epoxy $[\pm 45]_s$ laminate. Figure 7a shows the variation of stresses across the width at the $\pm 45°$ laminae interface, while 7b shows the variation of interlaminar shear through the thickness. As the number of segments is increased, the present solution approaches that for a laminate composed of homogeneous laminae. Since the true structure of a composite laminate lies between a model composed of homogeneous laminae and a model composed of discrete segments, the results of the two extreme models can serve to set the bounds for the actual stress field. These results are also applicable for laminates in which identical laminae are stacked adjacent to each other. As an example, the results for a $[45/45/-45/-45]_s$ laminate, using the present model, are identical to the case in which each lamina is idealized into two membrane segments (see Fig. 7). The peak interlaminar shear increases approximately thirty percent over the $[\pm 45]_s$ laminate and has a width of influence of approximately 10 lamina thicknesses, while the peak interlaminar shear for a $[45/-45/45/-45]_s$ laminate is approximately the same as that of the four layer $[\pm 45]_s$ laminate and has a width of influence of approximately 5 lamina thicknesses. Similar results are obtained for other fiber orientations. These results indicate that the interlaminar shear can be kept to a minimum by alternating the $+\beta$

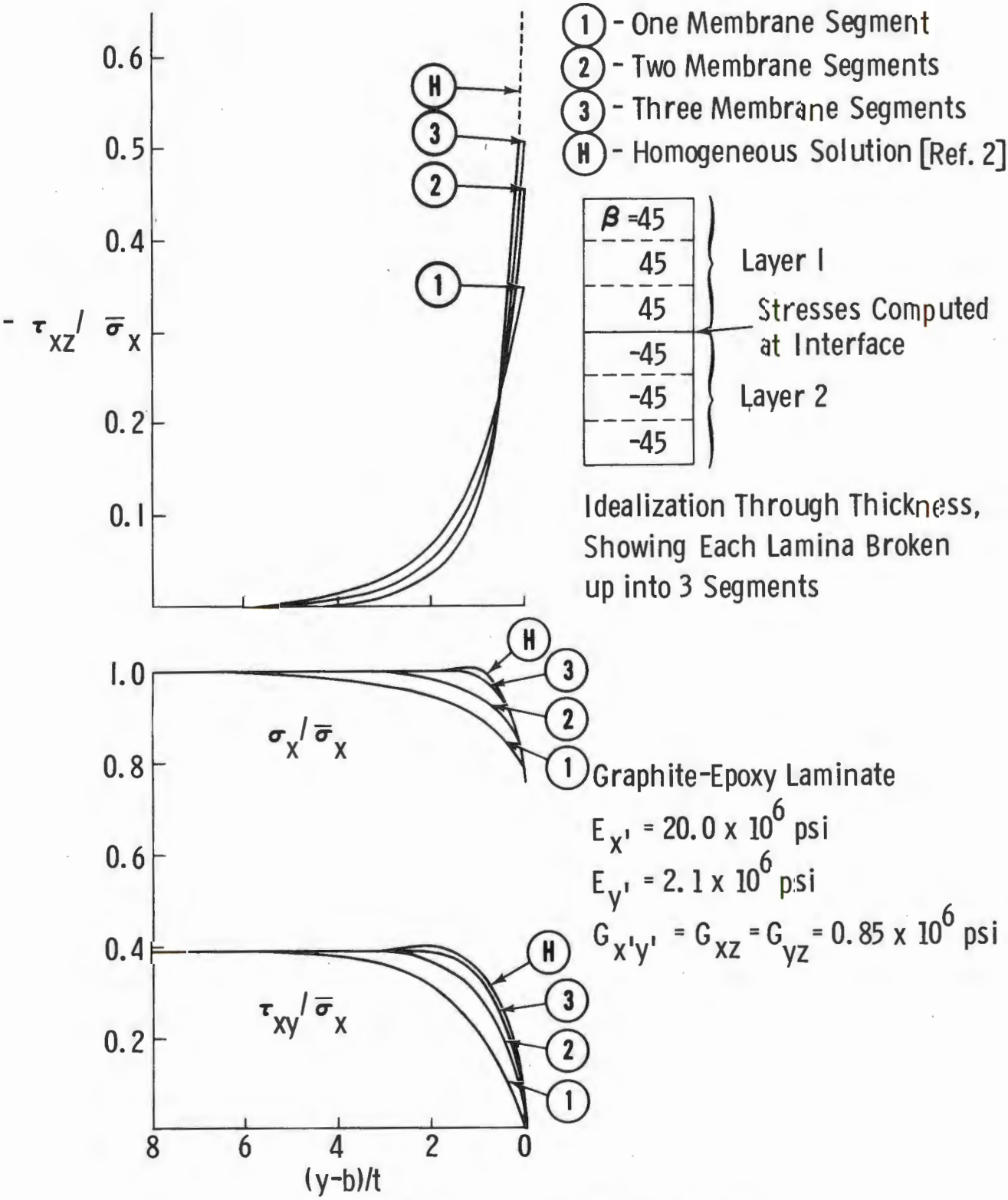

(a) Stress Distribution Across the Panel

Figure 7. Results for Various Lamina Models, $[\pm 45]_s$ Laminate.

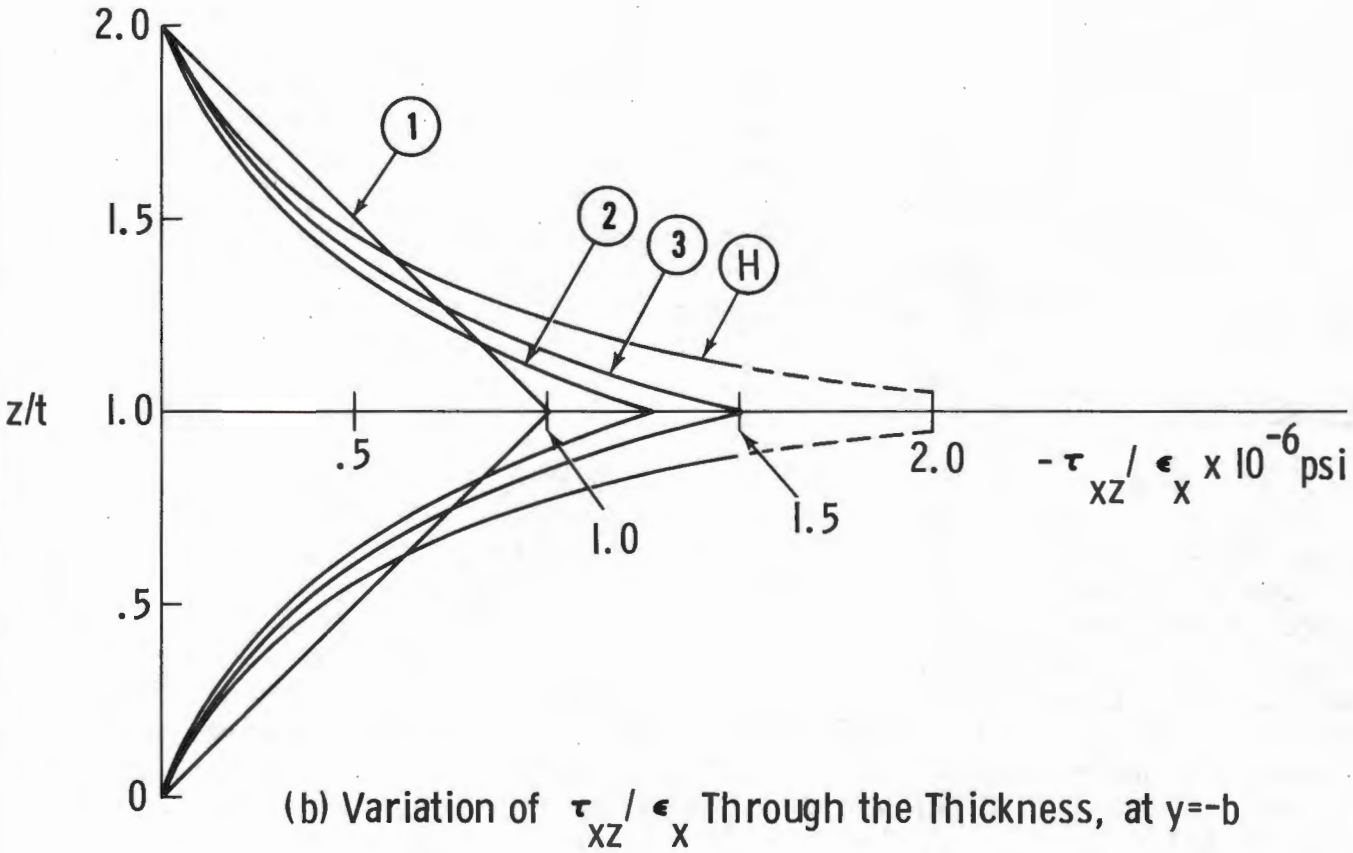

(b) Variation of τ_{xz}/ϵ_x Through the Thickness, at y=-b

Figure 7. Results for Various Lamina Models, $[\pm 45]_s$ Laminate (Cont)

and $-\beta$ laminae rather than stacking them together. For a laminate with identical adjacent laminae, e.g., a $[45_n/-45_n]_s$ laminate, the peak interlaminar shear stress increases with increasing n, having a limiting value given by the solution of a $[45/-45]_s$ laminate in which each lamina is considered as homogeneous.

In general there will be both normal and tangential interlaminar shear stresses except in a $[\pm \beta]_s$ laminate where only a tangential shear stress appears and in a $[0/90]_s$ laminate where only a normal stress appears. In Appendix B a closed form solution is obtained for a $[0/90]_s$ laminate using the methods of Ref. 1. This solution and the finite-element solution are in good agreement as shown in Fig. 8a. The finite-element solution does not allow the shearing stress normal to the free edge, τ_{yz}, to approach zero at the free edge; however, there is reason to believe that this may be a highly localized inaccuracy. This is indicated, to some extent, in Ref. 11 in which a double lap joint is analyzed. A closed form solution in which a zero shear condition is enforced at the free edge is compared with a finite-element solution, and the results are in excellent agreement except at the free edge.

Peel Stress

The normal or "peel" stress, σ_z, is not taken into account in the present model. This may be a shortcoming from two points: 1) the importance of predicting σ_z as it relates to strength predictions of composites and 2) the effect of its inclusion on the distributions of the other stress components. Reference 12 discusses the influence of the stacking sequence on laminate strength and concludes that interlaminar normal stress is a significant factor in the delamination of composites. This is based on mathematical arguments and reference to experimental results. The experiments cited (Refs. 13 and 14) deal with the comparison of a $[\pm 45/ \pm 15]_s$ with a $[\pm 15/ \pm 45]_s$ boron-epoxy laminate, and a $[90/0]_s$ with a $[0/90]_s$ glass-epoxy laminate, respectively. In each case the former laminate results in a higher strength, resulting from compressive normal stress near the free edge (Ref. 12). Other investigations (Refs. 15 and 16), however, have concluded that where thermal and/or mechanical stress causes matrix cracking between fibers in the laminate plane, matrix enhancement of fiber strength (above the dry bundle strength) through transfer of load from broken to unbroken fibers depends upon load paths through the thickness. For example, both a $[0/90]_s$ and a $[90/0]_s$ laminate experience transverse residual thermal strains

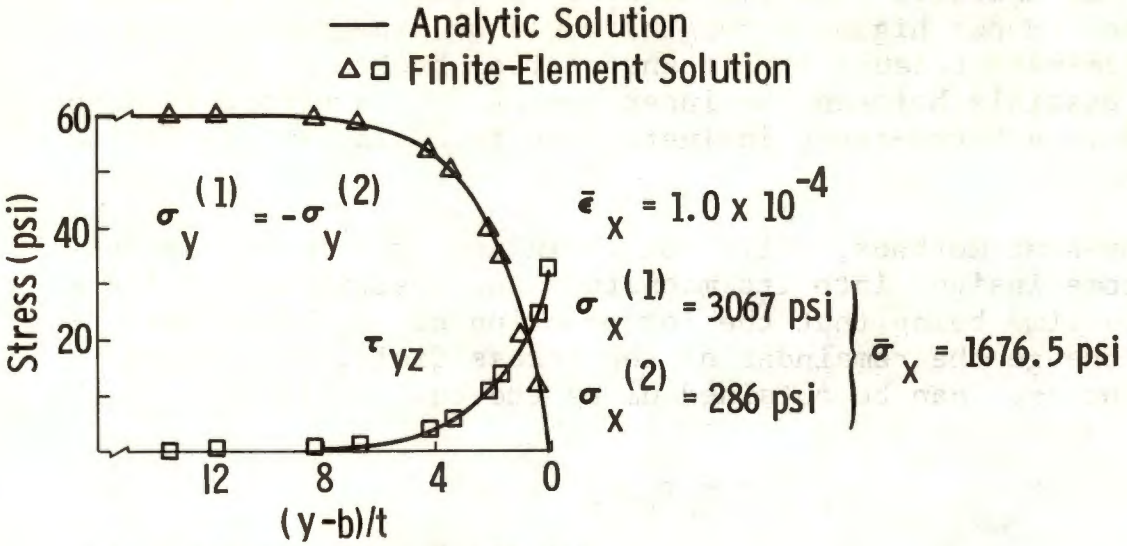

(a) Solution for Present Model

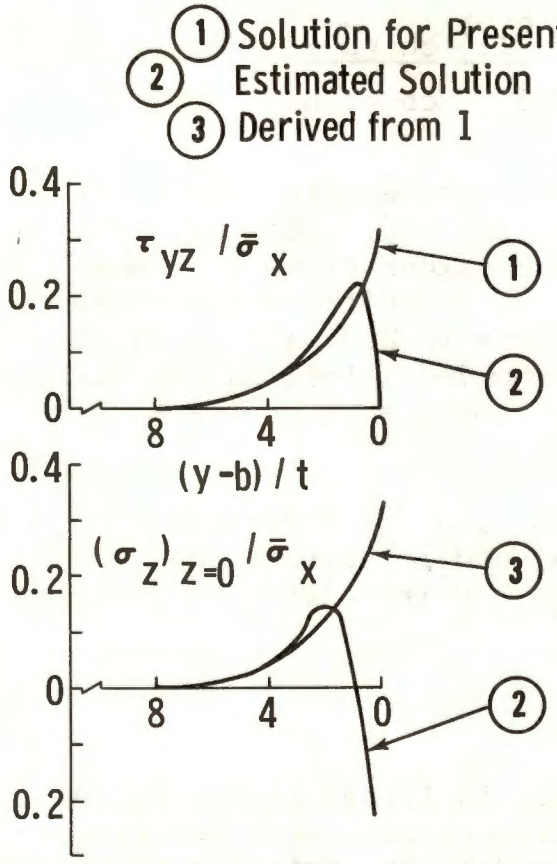

(b) Estimated Stresses with Inclusion of σ_z

Figure 8. Stress Distributions, $[0/90]_s$ Laminate

sufficient to initiate such cracks after cooling from the curing temperature. Hence higher strengths would be expected with the $[90/0]_s$ laminate because load transfer from broken to unbroken fibers is possible between the inner layers. This effect is more pronounced in a boron-epoxy laminate then in a glass-epoxy laminate (Ref. 16).

The present methods, while not including σ_z in the analysis, can give some insight into its magnitude and distribution. Assuming for the time being that the introduction of σ_z does not appreciably change the remainder of the stress field, then an expression for σ_z can be obtained using the equilibrium equation

$$\sigma_{z,z} = - \tau_{yz,y} \quad .$$

Using the results in Appendix B for a $[0/90]_s$ laminate, we find

$$(\sigma_z)_{z=0} = - 2 \frac{u^*}{a} Q_{12} G \frac{(Q_{22} - Q_{11})}{Q_{11} Q_{22}} \frac{\text{ch } \sqrt{\rho}\, y}{\text{ch } \sqrt{\rho}\, b} \quad ,$$

which is shown in Fig. 9b. Along with these results, qualitative curves representing the actual response for τ_{yz} and σ_z are shown. These are based on equilibrium considerations as demonstrated in Ref. 12. The inclusion of σ_z results in a reduction of peak interlaminar shear stress as shown in Ref. 11, which discusses this very issue with respect to bonded joints in composite materials. For comparison a $[0/90]_s$ laminate is analyzed, with the inclusion of σ_z, in Ref. 17.

A qualitative determination of σ_z and its effect on the other stress components is predictable, and it appears that the need for an exact determination of σ_z, as it relates to strength predictions, is open to question.

Panel With a Cutout

A flat panel with a circular cutout is loaded along two opposite edges. The dimensions of the panel are such that the stress field around the cutout is not influenced by the external boundaries. A typical idealization is shown in Fig. 9, which contains 223 members and 138 nodes. Results for a $[\pm 45]_s$ laminate, where the ratio of hole radius to lamina thickness is 100, are shown in

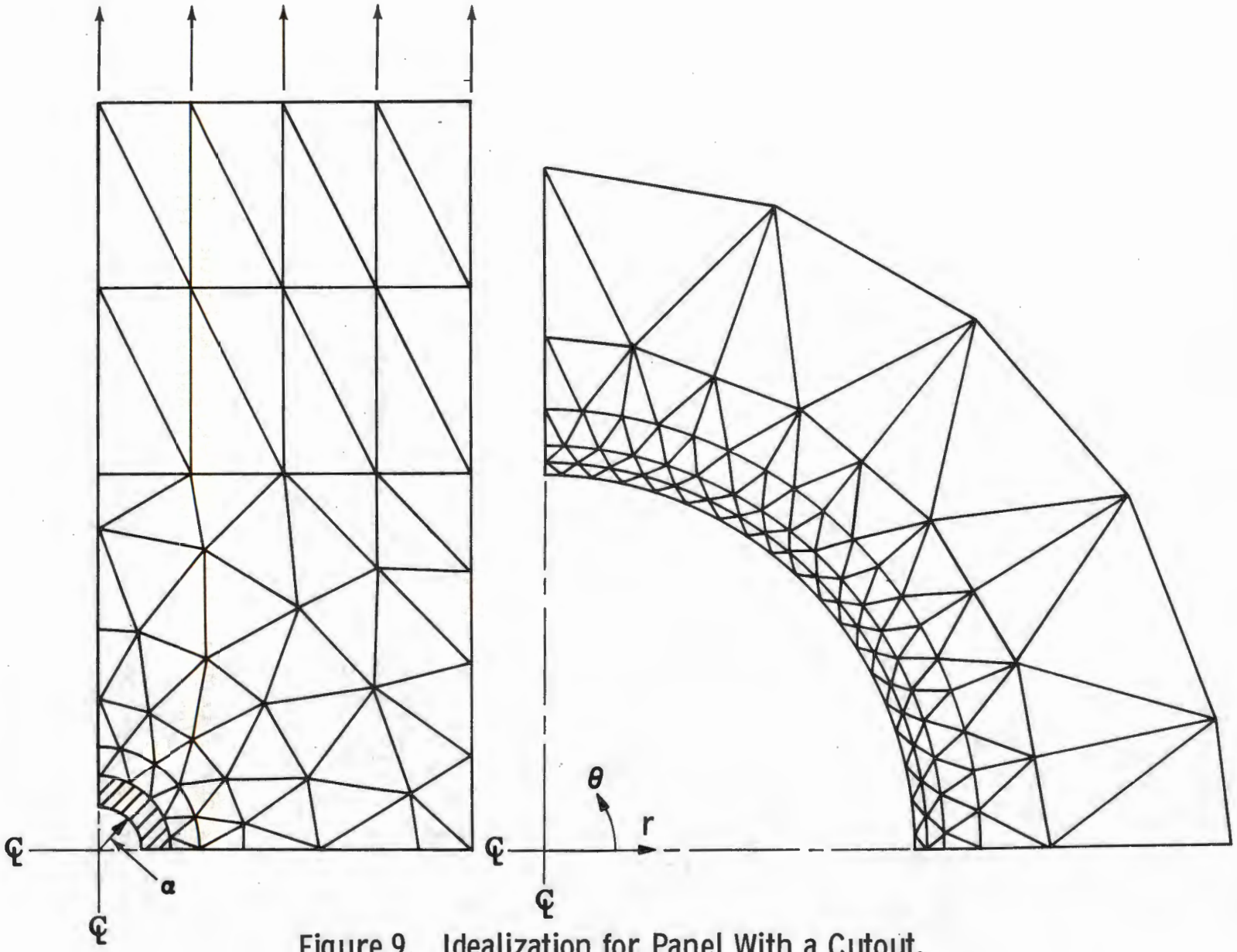

Figure 9. Idealization for Panel With a Cutout.

Fig. 10. To test the finite-element idealization, a comparison is made between the finite-element solution and exact solution of the mean circumferential stress at a distance slightly away from the cutout (Fig. 10a). These results are in excellent agreement. The inclusion of interlaminar shear causes the mean circumferential stress to deviate from the classical case, this deviation being most pronounced in the regions of high circumferential interlaminar shear, $\tau_{\theta z}$. The radial interlaminar shear stress is small compared with the circumferential interlaminar shear stress. This is true for all values of β. Along the radial coordinates $\theta = 0°$ and $\theta = 90°$, where the fiber orientations are either $\pm 45°$ or $\mp 45°$ when measured from these axes, the stress field behaves in a manner similar to that along a free edge of a $[\pm 45]_s$ rectangular panel. The straight edge solution of a $[\pm 45]_s$ laminate yields $\sigma_x/\sigma_{xa} = 0.86$ and $\tau_{xz}/\sigma_{xa} = 0.28$, where σ_{xa} is the classical normal stress at the point. The corresponding values at the edge of the cutout along $\theta = 0°$ are 0.89 and 0.26 and along $\theta = 90°$ are 0.88 and 0.27, respectively. The reason for the deviation between these results and those along the straight edge is that the interlaminar shear deformation edge effect emanates from points along a boundary and extends over a distance equal to the width of influence. Therefore a "circle of influence" exists around each point in which the stress distribution influences the stress behavior at that point. Along a straight boundary of infinite length, the stresses within the circle of influence are uniform in a direction tangent to the boundary. Along the edge of a cutout, however, the stress field is not uniform in the circumferential direction. As the radius of the hole increases, the stress field within the circle of influence approaches a uniform state, and the resulting stress field at a point approaches that of a straight edge solution. Figure 11 shows the resulting interlaminar shear for a $[\pm 45]_s$ laminate as the ratio of hole radius to laminate thickness is varied. The straight edge solution is approached at the axes within 5 percent when the ratio of hole radius to laminate thickness equals 100, and within 20 percent when the ratio equals 10. As the ratio of hole radius to lamina thickness decreases, the interlaminar shear stress flattens out as a function of θ and decreases in average value.

Figure 12 shows results for a $[\pm 30]_s$ laminate. The values of $\sigma_\theta/\sigma_{\theta a}$ and $\tau_{\theta z}/\sigma_{\theta a}$ ($\sigma_{\theta a}$ is the classical mean circumferential stress at the point) along the cutout at $\theta = 0°$ and $\theta = 90°$ for a ratio of $a/t = 100$ is similar to the corresponding values of stress along the straight edge of a $[\pm 30]_s$ and $[\pm 60]_s$ laminate, respectively. Note the significant reduction of stress

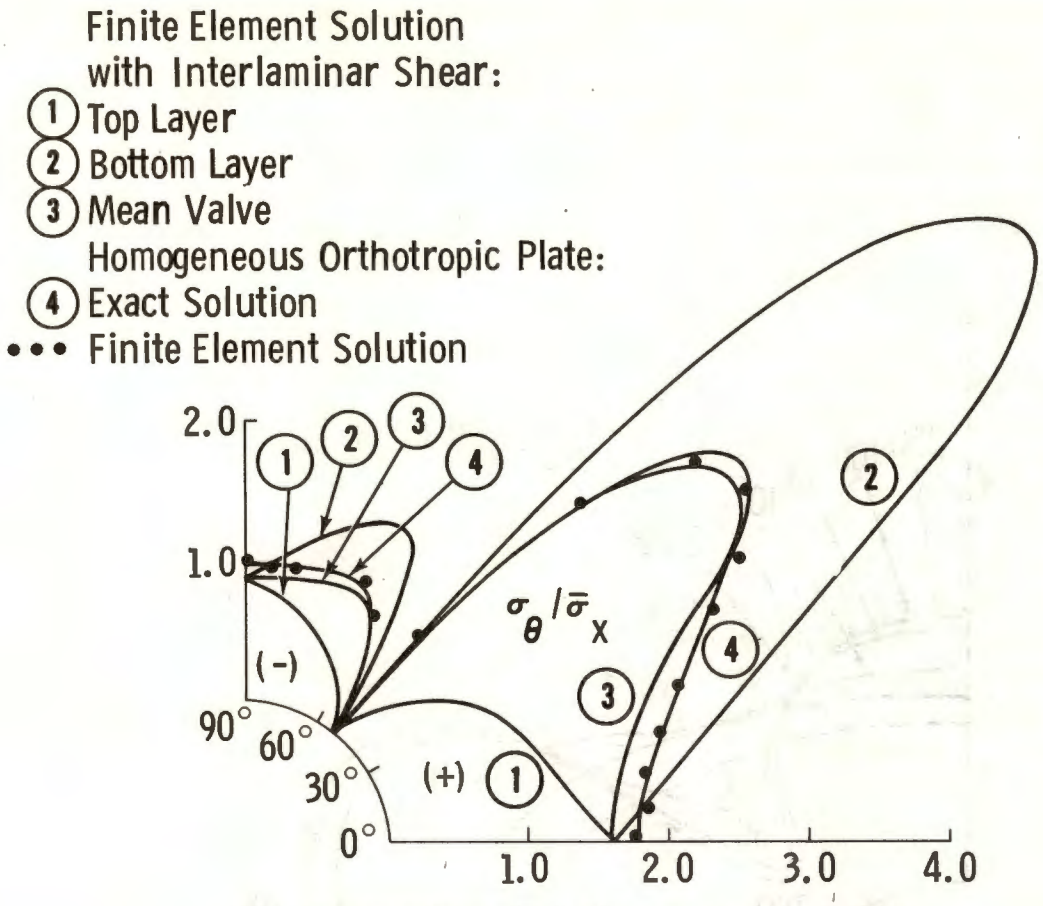

(a) Circumferential Stress at r/a = 1.007

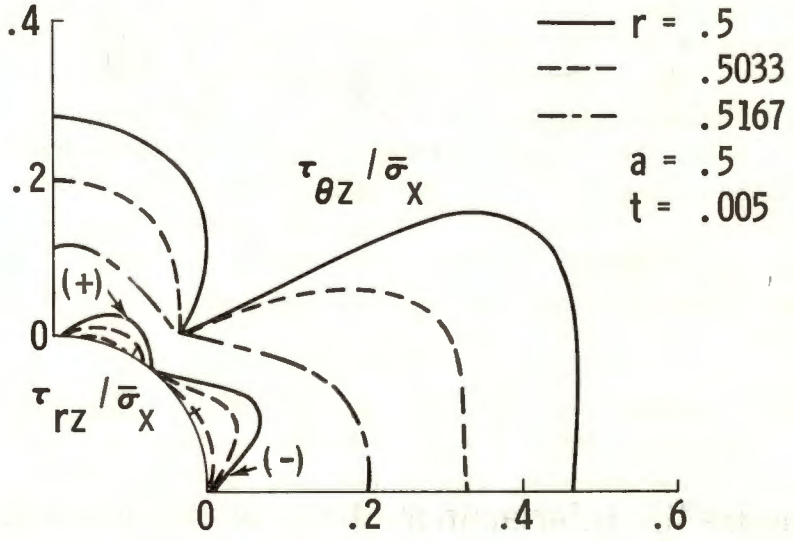

(b) Interlaminar Shear Stresses

Figure 10, Stresses Around Cutout, $[\pm 45]_s$ Laminate

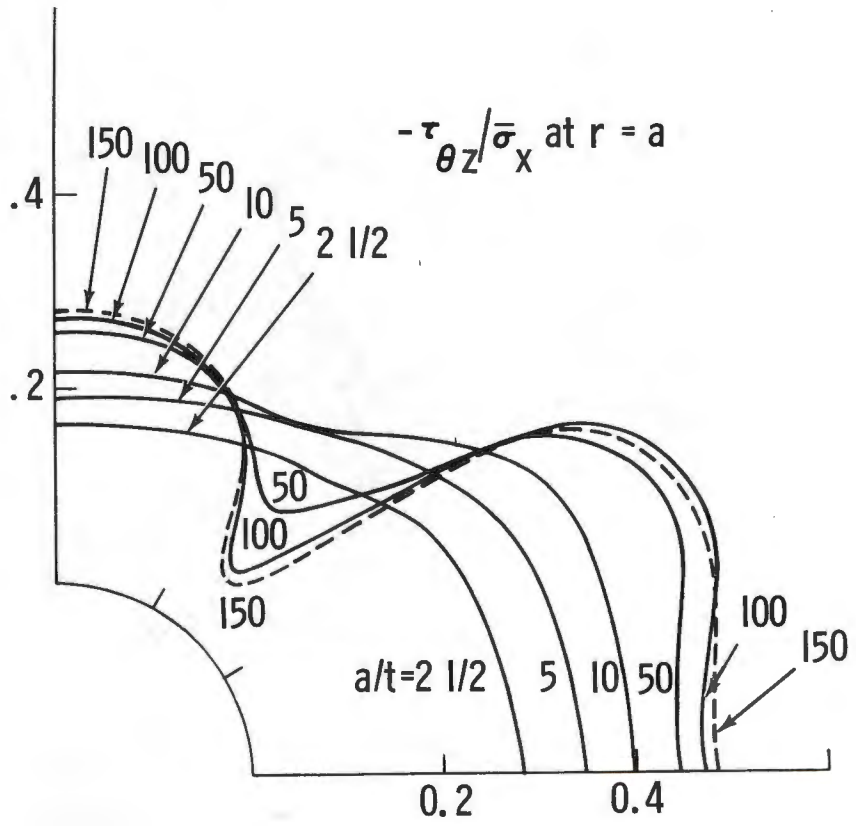

Figure 11. Interlaminar Stress Distributions for Various Radius to Thickness Ratios, $[\pm 45]_s$ Laminate.

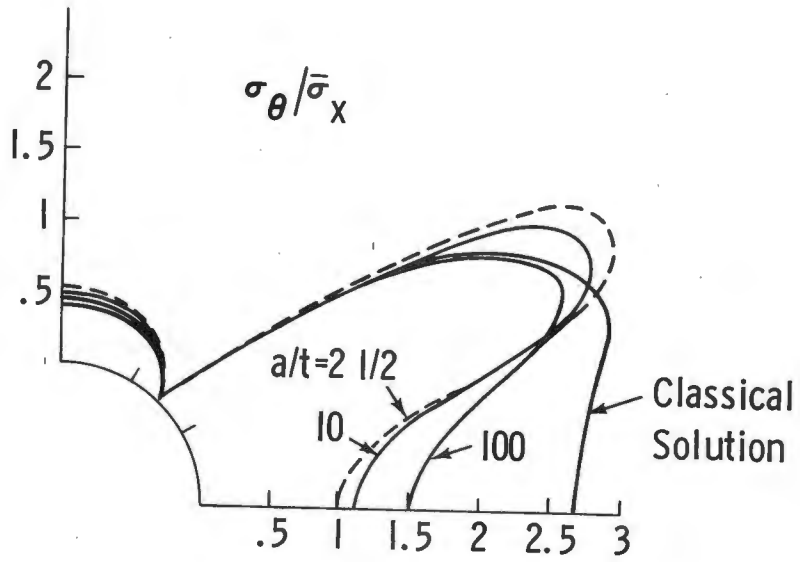

(a) Mean Circumferential Stress at r/a=1.007

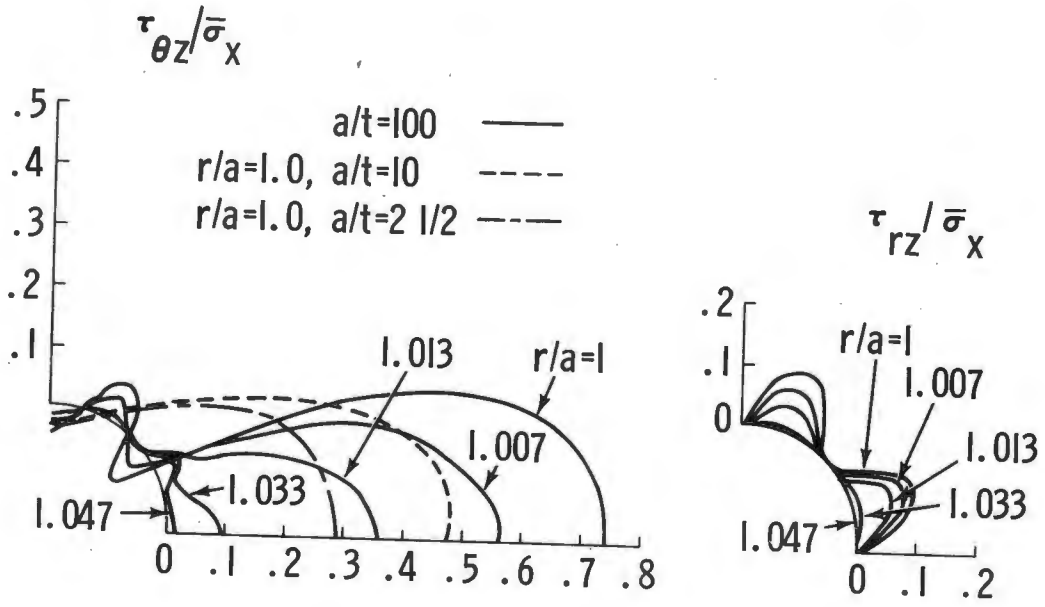

(b) Interlaminar Shear Stresses

Figure 12. Stress Distributions Around Cutout, $[\pm 30]_s$ Laminate.

concentration in σ_θ at $\theta = 0°$ and the redistribution of $\tau_{\theta z}$ and σ_θ for the cases in which the radius to lamina thickness is reduced. The reduction in stress concentration in σ_θ at $\theta = 0°$ is predictable from the straight edge solution of a $[\pm 30]_s$ laminate.

Results for a $[0/90]_s$ laminate containing a circular cutout are shown in Fig. 13. There is little variation of σ_θ from the classical solution along the $\theta = 0°$ and $\theta = 90°$ axes. This is similar to the straight edge solution for a $[0/90]_s$ laminate where there is little diffusion of the axial stress due to interlaminar shear. The circumferential interlaminar shear is zero along $\theta = 0°$ and $\theta = 90°$, as expected, but grows rapidly away from these points, and is greater in magnitude than the maximum radial interlaminar shear stress. Unlike the behavior in a $[\pm \beta]_s$ laminate, the circumferential stress varies rapidly in the circumferential direction near $\theta = 90°$ and in both the circumferential and radial directions near $\theta = 0°$. This accounts for the difference in radial interlaminar shear stress between the results along $\theta = 0°$ and $\theta = 90°$ and those along a straight edge of a $[0/90]_s$ laminate. Of interest is the radial interlaminar shear growth along $\theta = 90°$ and change of direction along $\theta = 0°$ when the ratio of hole size to lamina thickness decreases. This is in contrast to the steady decrease of circumferential interlaminar shear around the cutout as a/t decreases.

V. INELASTIC RESULTS

The method of initial strains to describe the inelastic behavior is briefly described in Section III. In this first study of the problem, it is assumed that the interlaminar matrix material can deform plastically while the in-plane material behavior is assumed to be elastic throughout the entire load history.

The interlaminar stress strain behavior of boron-epoxy is shown in Fig. 14, along with its Ramberg-Osgood parameters. Stresses are computed for a $[\pm 45]_s$ boron-epoxy laminate at a load level 4.22 times that at which yielding begins ($\tau_y = 3460$ psi). Compared to the elastic response at the same load level, the interlaminar shear stress is lower near the edge and is slightly higher at points more remote from the edge, but it does not extend over a significantly greater region. Moreover, the effect of the nonlinearity on the membrane stresses is slight (Fig. 15).

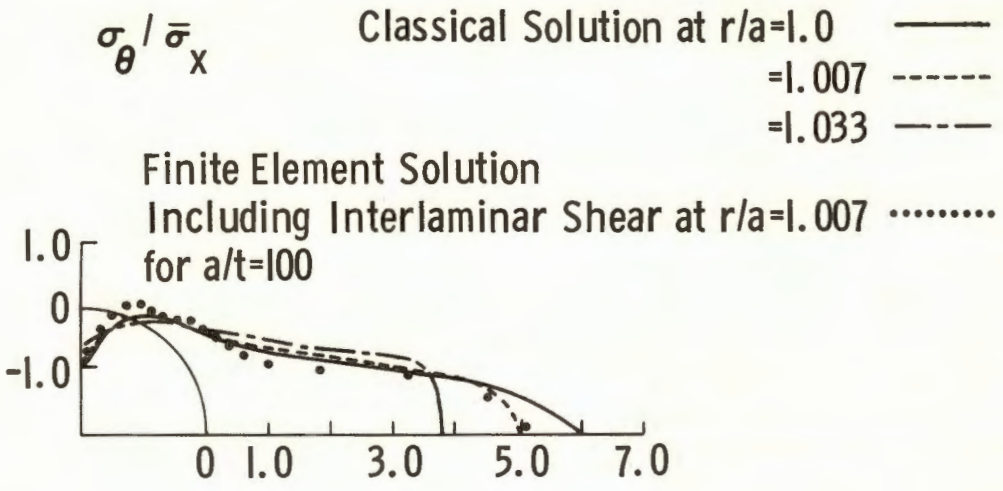

(a) Mean Circumferential Stress

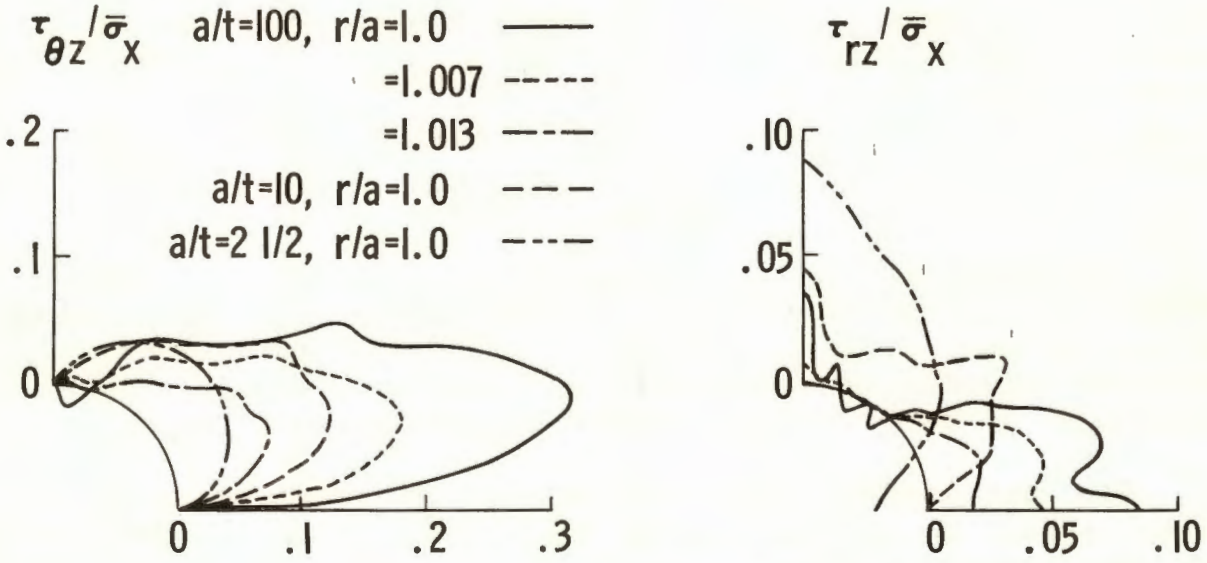

(b) Interlaminar Shear Stresses

Figure 13. Stress Distribution Around Cutout, $[0/90]_s$ Laminate.

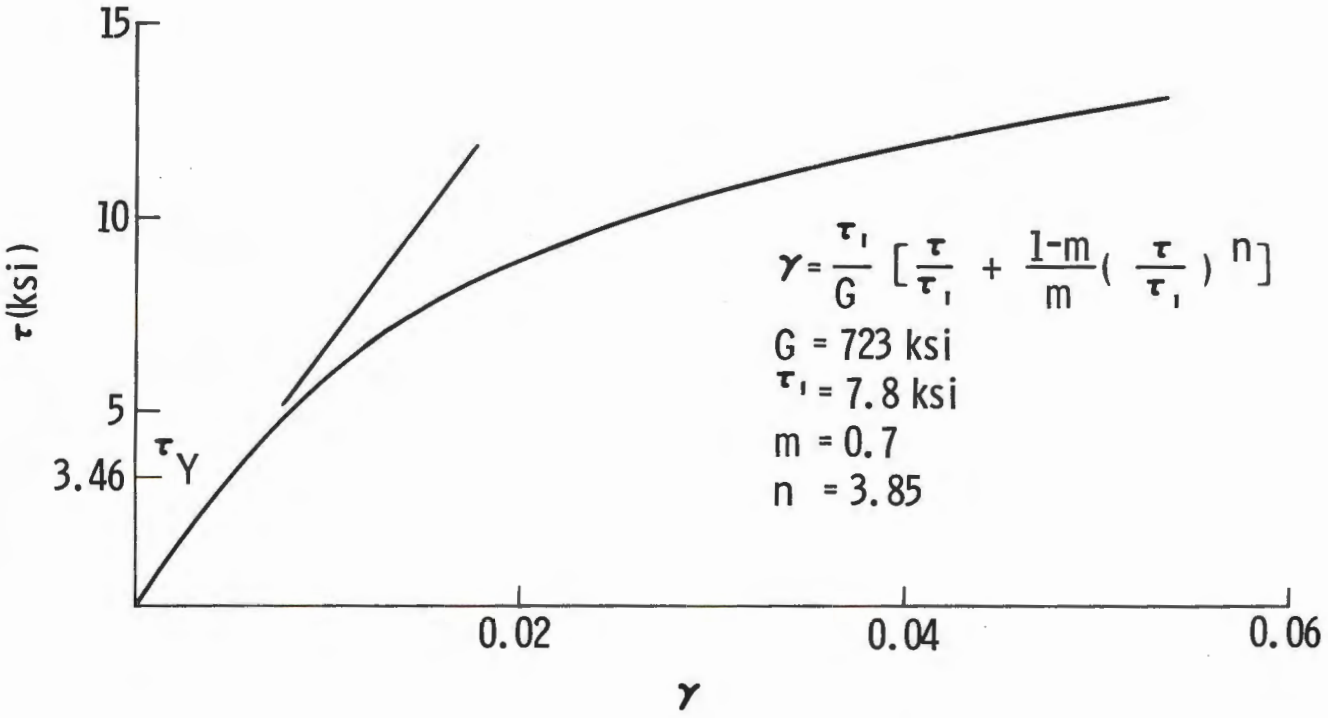

Figure 14. Interlaminar Shear Stress-Strain Curve and Ramberg-Osgood Parameters for Boron-Epoxy Laminate.

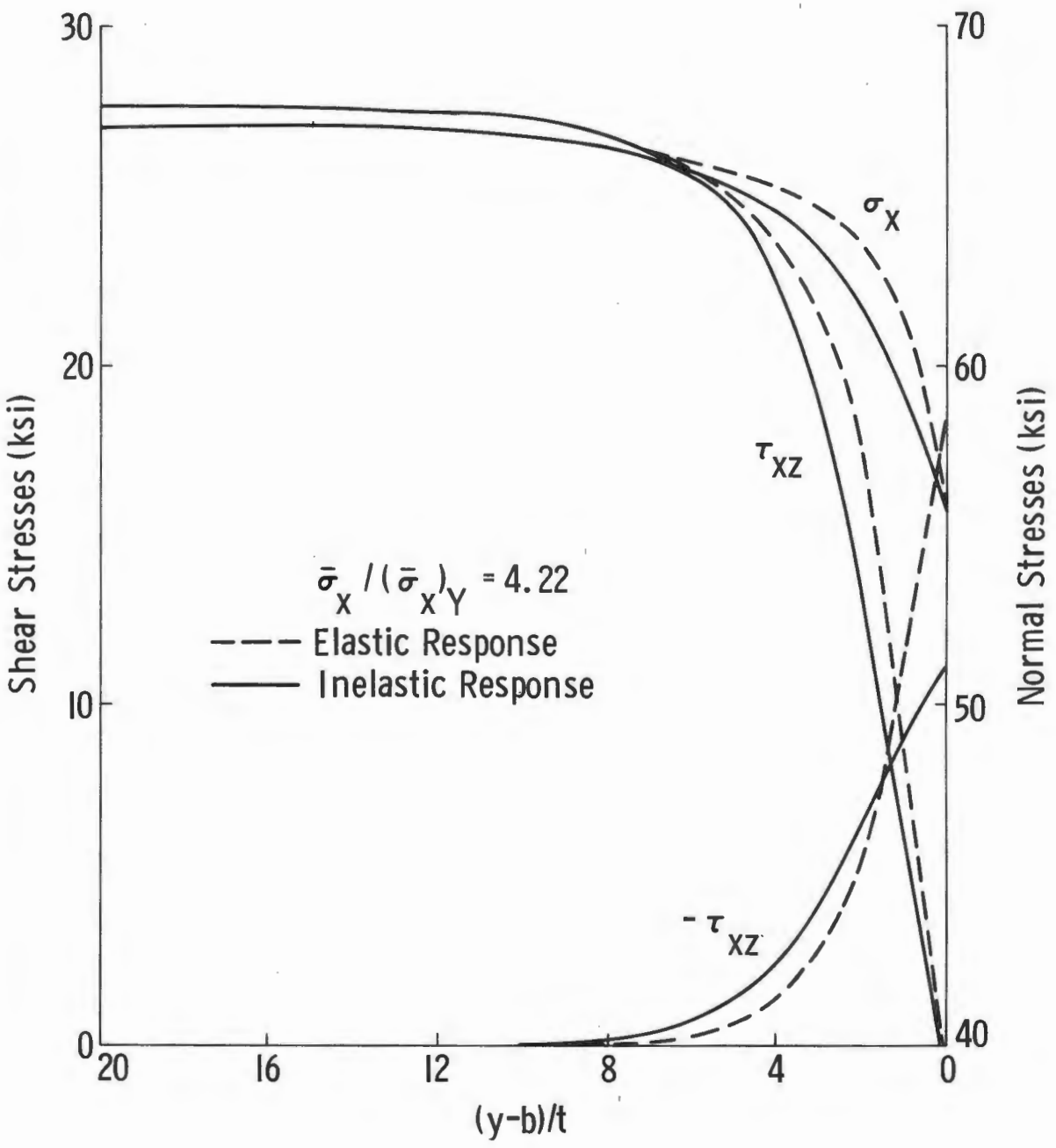

Figure 15. Comparison of Elastic and Inelastic Response, $[\pm 45]_s$ Laminate.

A multilayered $[0/\pm45/0/\bar{90}]_s$ boron-epoxy laminate is analyzed. The "loaded edge" displacements are increased until a tensile load of 112 ksi is reached (slightly greater than the expected fracture stress). The load is then decreased to a compressive load of 112 ksi and finally brought back to zero. In general, similar results are obtained during tensile loading of a $[\pm 45]_s$ laminate, i.e., a reduction in peak interlaminar shear stresses and little change in the membrane stresses are observed. The interlaminar shear components (in the layers in which they have the greatest peak magnitude) at a distance of 0.1 laminate thickness from the $y = - b$ edge are plotted in Fig. 16 for the complete loading cycle. Of interest is the buildup of residual shearing stresses that occurs for both components of interlaminar shear. The mean stress, $\bar{\sigma}_x$, varies linearly with respect to the applied displacement to within five percent, an indication that the interlaminar shear nonlinearity has little effect on the gross laminate behavior. Interlaminar shear stresses around a circular cutout in a $[\pm 45]_s$ laminate are shown in Fig. 17. High residual shearing stresses occur in the vicinity of $\theta < 45°$, and relatively low residual shearing stresses occur for $\theta > 45°$.

VI. DISCUSSION

A finite element program was developed for the study of interlaminar shear deformation in composite laminates. The main building block of this program, called COMPEL, is the COMPosite ELement, which is described in Appendix A. The displacement method is used and the solution is effected by the use of a Cholesky decomposition scheme. Typical running times are 29 sec (elastic) and 1.2 sec per increment (plastic) for an idealization containing 210 degrees of freedom with a mean bandwidth of 132.

The following observations pertain to the techniques used in analyzing a composite laminate with the use of the present composite element:

- To determine accurately the interlaminar shear stresses, values of $t/\bar{c} > 1$ must be observed in the construction of a finite-element idealization.

- Upper and lower bounds for interlaminar shear stresses can be found by varying the number of idealized segments through the thickness.

- A qualitative determination of the "peel stress," σ_z, and its effect on the other stress components is predictable.

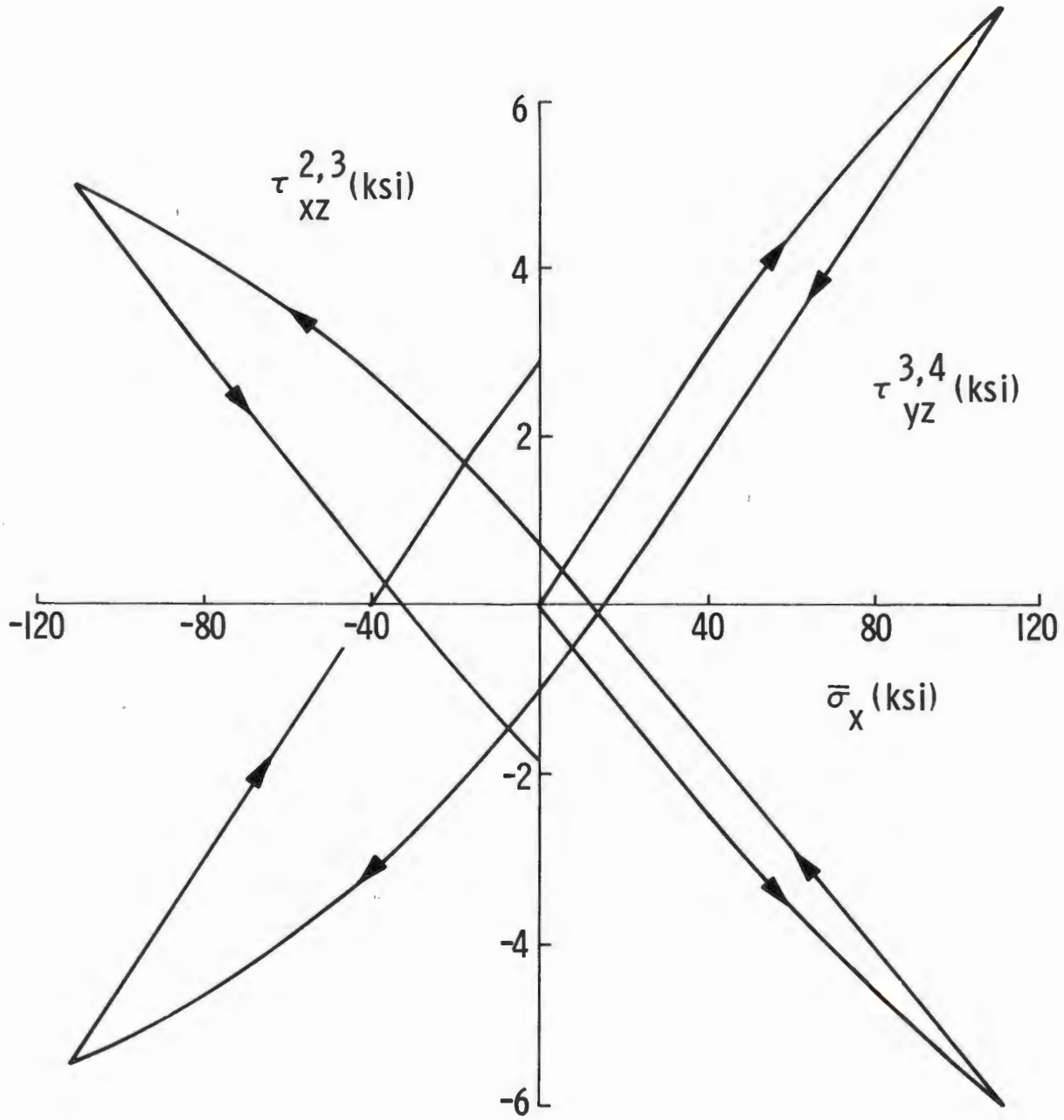

Figure 16. Interlaminar Shear Stresses at $(y-b)/t=0.4$ for Cyclic Loading, $[0/\pm45/0/\bar{90}]_s$ Laminate.

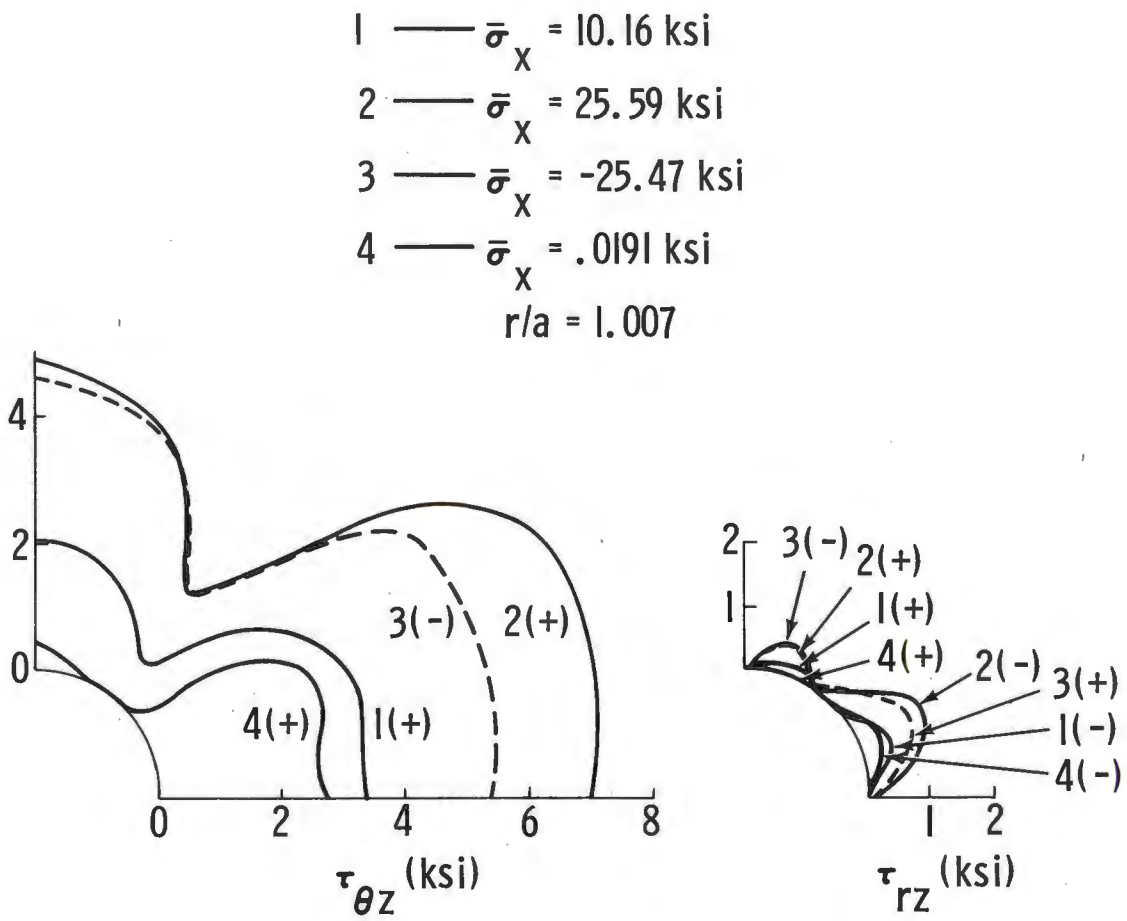

Figure 17. Interlaminar Shear Stresses Around Cutout for Cyclic Loading, $[\pm 45]_s$ Laminate.

The following results pertain to the elastic response of a composite laminate:

- The stacking sequence is the dominant factor in controlling the interlaminar shear region; e.g., alternating $+\beta$ and $-\beta$ laminae keeps the peak interlaminar shear stress and width of influence to a minimum.

- For a laminate with identical adjacent laminae, e.g., a $[45_n/\text{-}45_n]_s$ laminate, the peak interlaminar shear stress increases with increasing n, having a limiting value corresponding to a four-ply $[45/\text{-}45]_s$ laminate in which each lamina is considered as homogeneous.

- Around a circular cutout the circumferential interlaminar shear stress component tends to be of greater magnitude than the radial component for all stacking sequences, the exception being in the region between $0°$ and $90°$ laminae, where a higher radial component occurs for small values of a/t.

- For a circular cutout, as the ratio of hole radius to lamina thickness decreases, the interlaminar shear stresses flatten out, as a function of θ, and decrease in average value, except in the case noted above.

The results pertaining to the inelastic interlaminar shear behavior show:

- High residual interlaminar shear stresses develop during cyclic loading.

- Interlaminar shear nonlinearity has little effect on the gross laminate behavior.

This study accounts only for the plastic deformation of the interlaminar matrix material. Accounting for the most general state of plastic deformation requires that the analysis provide the capability to include a criterion to predict the occurrence of failure for a particular stress state in an orthotropic lamina under combined stress and a technique that can adequately represent the subsequent phenomenological behavior upon further loading. The first requirement, i.e., defining an acceptable fracture or yield criterion, has been the subject of a large number of studies (see Ref. 18 for an extensive bibliography). These approaches usually

provide an analytical expression, referred to as "interaction formulas," representing a quadratic surface in stress space, which best fits some experimental data for a given material. Although the reliability of the various criteria available is not established and in some cases is open to question, one can choose the "best" criterion for a particular material and readily incorporate such into an analysis until a "better" one becomes available. Methods to treat the behavior of the material beyond initial failure or yielding have been studied and appear in Refs. 19-21. In Ref. 19 the elastic stiffness properties of the structure are modified to reflect the development of nonlinear material behavior. In Refs. 20 and 21 prescribed conditions are imposed on the subsequent behavior of the stress components, i.e., set to zero (Ref. 20) or required to follow a unidirectional nonlinear relation (Ref. 21). As indicated in Ref. 22, these approaches to predict laminate strength represent a good beginning but require further work. Efforts toward the goal of providing a meaningful description of a general inelastic strength analysis represent a logical extension of the work here presented.

VII. REFERENCES

1. Puppo, A. H. and Evensen, H. A., "Interlaminar Shear in Laminated Composites under Generalized Plane Stress," J. Comp. Materials, Vol. 4, p. 204, 1970.

2. Pipes, R. B. and Pagano, N. J., "Interlaminar Stresses in Composite Laminates under Uniform Axial Extension," J. Comp. Materials, Vol. 4, p. 583, 1970.

3. Isakson, G. and Levy, A., "Finite-Element Analysis of Interlaminar Shear in Fibrous Composites," J. Comp. Materials, Vol. 5, p. 273, 1971.

4. Zienkiewicz, O. C., The Finite Element Method in Structural and Continuum Mechanics, McGraw-Hill, p. 32, 1967.

5. Armen, H., Pifko, A., and Levine, H. S., Finite Element Analysis of Structures in the Plastic Range, NASA Contractor's Report CR-1649, February 1971.

6. Isakson, G., Armen, H., and Pifko, A., Discrete-Element Methods for the Plastic Analysis of Structures, NASA Contractor's Report CR-803, October 1967.

7. Havner, K. S., "On Convergence of Iterative Methods in Plastic Strain Analysis," J. Solid Structures, Vol. 4, p. 491, 1968.

8. Prager, W., "A New Method of Analyzing Stress and Strains in Work-Hardening Plastic Solids," J. Appl. Mech., Vol. 23, p. 493, 1956.

9. Ziegler, H., "A Modification of Prager's Hardening Rule," Quart. Appl. Math., Vol. 17, No. 1, p. 55, 1959.

10. Walz, J. E., Fulton, R. E., and Cyrus, N. J., "Accuracy and Convergence of Finite Element Approximations," Proceedings of the Second Conference on Matrix Methods in Structural Mechanics, Wright-Patterson Air Force Base, Ohio, 15-17 October 1968.

11. Fehrle, A. C. et al., Lockheed-Georgia Company, Marietta, Georgia, Development of an Understanding of the Fatigue Phenomena of Bonded and Bolted Joints in Advanced Filamentary Composite Materials, Technical Report AFFDL-TR-71-44, Air Force Flight Dynamics Laboratory, Air Force Systems Command, Wright-Patterson Air Force Base, Ohio, June 1971.

12. Pagano, N. J. and Pipes, R. B., "The Influence of Stacking on Laminate Strength," J. Comp. Materials, Vol. 5, p. 50, January 1971.

13. Foye, R. L. and Baker, D. J., "Design of Orthotropic Laminates," presented at the 11th Annual AIAA Structures, Structural Dynamics, and Materials Conference, Denver, Colorado, April 1970.

14. Kaminski, B. E., "On the Determination of the Failure Surface for an Orthotropic Quasi-Homogeneous Material," Master's Thesis, Georgia Institute of Technology, June 1969.

15. Tsai, S. W. et al., Effect of Constituent Material Properties on the Strength of Fiber-Reinforced Composite Materials, Technical Report AFML-TR-66-190, August 1966.

16. Hadcock, R. N., "Strength of Multidirectional Boron-Epoxy Laminates," Proceedings of SPI 24th Annual Technical Conference, Soc. of the Plastics Industry, Washington, D.C., February 1969.

17. Rybicki, E. F., "Approximate Three-Dimensional Solution for Symmetric Laminates Under Inplane Loading," J. Comp. Materials, Vol. 5, p. 354, July 1971.

18. Puppo, A. H. and Evensen, H. A., "Strength of Anisotropic Materials under Combined Stresses," presented at AIAA/ASME 12th Structures, Structural Dynamics and Materials Conference, Anaheim, California, April, 1971, paper 71-368.

19. Tsai, S. W., Strength Characteristics of Composite Materials, NASA CR-224, 1965.

20. Petit, P. H. and Waddoups, M. E., "A Method of Predicting the Non-Linear Behavior of Laminated Composites," J. Comp. Materials, Vol. 3, p. 2, 1969.

21. Rosen, B. W. and Dow, N. F., "Mechanics of Failure of Fibrous Composites," in Fracture, Vol. VII, H. Liebowitz, ed., Academic Press, 1970.

22. Rosen, B. W., "Structural Composites - Design and Analysis," Second Annual Structures Design Lecture presented at AIAA/ASME 12th Structures, Structural Dynamics and Materials Conference, Anaheim, California, April, 1971.

ACKNOWLEDGMENT

The authors gratefully acknowledge the work of Joseph S. Miller in programming the analysis.

APPENDIX A

FORMULATION OF STIFFNESS MATRICES

The elastic strain energy is expressed as

$$U = \frac{1}{2}\int_V \underset{\sim}{\sigma}'\underset{\sim}{\epsilon} dV \quad . \tag{A-1}$$

The elastic strains are written in terms of the total and plastic strains as

$$\underset{\sim}{\epsilon} = \underset{\sim}{\epsilon}_t - \underset{\sim}{\epsilon}_p \quad , \tag{A-2}$$

where, for present purposes, all components of total and plastic strains are assumed constant within an element. The constant strains are represented in the following form:

$$\begin{aligned} \underset{\sim}{\epsilon}_p &= \underset{\sim}{\epsilon}_o \\ \underset{\sim}{\epsilon}_t &= \underset{\sim}{W}\,\underset{\sim}{u} \quad , \end{aligned} \tag{A-3}$$

where $\underset{\sim}{\epsilon}_o$ are the centroidal plastic strains, $\underset{\sim}{u}$ are the nodal displacements, and $\underset{\sim}{W}$ represents the matrix of coefficients associated with the strain-nodal displacement relations. By using the elastic stress-strain relation

$$\underset{\sim}{\sigma} = \underset{\sim}{C}\,\underset{\sim}{\epsilon} \tag{A-4}$$

and Eq. (A-2), Eq. (A-1) becomes

$$U = \frac{1}{2}\int_V (\underset{\sim}{\epsilon}_t - \underset{\sim}{\epsilon}_p)'\,\underset{\sim}{C}(\underset{\sim}{\epsilon}_t - \underset{\sim}{\epsilon}_p) dV \quad .$$

From a consistent energy approach, or equivalently from the application of the principle of virtual work, the following equation is arrived at:

$$\underset{\sim}{f} = \underset{\sim}{k}\,\underset{\sim}{u} - \underset{\sim}{k}_p\underset{\sim}{\epsilon}_o \tag{A-5}$$

where

$$\underset{\sim}{k} = \int_V \underset{\sim}{W}' \underset{\sim}{C} \underset{\sim}{W} dV$$

$$\underset{\sim}{k}_p = \int_V \underset{\sim}{W}' \underset{\sim}{C} dV \quad . \tag{A-6}$$

These general principles are applied to the specific element model outlined in the text and shown in Fig. 2, and it is found that the contribution to the stiffness matrices, expressed in Eqs. (A-6), of each of the two components of the heterogeneous material, viz., the in-plane fiber-matrix and interlaminar matrix segments, is uncoupled. The total strains, $\underset{\sim}{\epsilon}_t$, are represented in the form

$$\underset{\sim}{\epsilon}_t = (\underset{\sim}{\epsilon}_m \underset{\sim}{\gamma}) \quad ,$$

where $\underset{\sim}{\epsilon}_m$ contains the in-plane membrane strain components, ϵ_x, ϵ_y, and γ_{xy}, and $\underset{\sim}{\gamma}$ contains the interlaminar shearing strains γ_{xz}, γ_{yz}. To derive the stiffness matrices for an individual element explicitly, a notation that describes the contribution of the various segments is used. This is shown for the strain components and elsewhere, when necessary for clarity. The strain components are denoted as

$$\underset{\sim}{\epsilon}_m = (\underset{\sim}{\epsilon}_m^1 \; \underset{\sim}{\epsilon}_m^2 \; \ldots \; \underset{\sim}{\epsilon}^n)$$

$$\underset{\sim}{\gamma} = (\underset{\sim}{\gamma}^{1,2} \; \underset{\sim}{\gamma}^{2,3} \; \ldots \; \underset{\sim}{\gamma}^{n-1,n}) \quad ,$$

where n is the number of layers, and

$$\underset{\sim}{\epsilon}_m^i = (\epsilon_x^i \; \epsilon_y^i \; \gamma_{xy}^i)$$

$$\underset{\sim}{\gamma}^{i,j} = (\gamma_{zx}^{i,j} \; \gamma_{zy}^{i,j}) \quad ,$$

in which a single superscripted quantity, say ϵ_x^i, denotes an in-plane property associated with layer i, and a double superscripted

quantity, say $\gamma_{zx}^{i,j}$, denotes an interlaminar property associated with the matrix region between layers i and j.

The total strain-displacement relation, Eq. (A-3), is expressed as

$$\begin{pmatrix} \underset{\sim}{\epsilon}_m \\ \underset{\sim}{\gamma} \end{pmatrix} = \begin{pmatrix} \underset{\sim}{W}_m \\ \underset{\sim}{W}_s \end{pmatrix} \underset{\sim}{u} \quad . \tag{A-7}$$

Conforming to the outline notation,

$$\underset{\sim}{W}_s = \begin{pmatrix} \underset{\sim}{W}_s^{1,2} & & & \\ & \underset{\sim}{W}_s^{2,3} & & \\ & & \ddots & \\ & & & \underset{\sim}{W}_s^{n-1,n} \end{pmatrix} , \quad \underset{\sim}{W}_m = \begin{pmatrix} \underset{\sim}{W}_m^{1} & & & \\ & \underset{\sim}{W}_m^{2} & & \\ & & \ddots & \\ & & & \underset{\sim}{W}_m^{n} \end{pmatrix}$$

and

$$\underset{\sim}{u} = (\underset{\sim}{u}^1 \ \underset{\sim}{u}^2 \ \ldots \ \underset{\sim}{u}^n)$$

where

$$\underset{\sim}{u}^n = (u_i^n v_i^n u_j^n v_j^n u_k^n v_k^n) \quad ,$$

subscripts denoting nodal points, and,

$$\underset{\sim}{W}_s^{i,j} = \begin{bmatrix} 1 & 0 & 1 & 0 & 1 & 0 & -1 & 0 & -1 & 0 & -1 & 0 \\ 0 & 1 & 0 & 1 & 0 & 1 & 0 & -1 & 0 & -1 & 0 & -1 \end{bmatrix} / 3t^{i,j} \quad ,$$

with $t^{i,j}$ representing the thickness. The quantities associated with the triangular in-plane orthotropic layers are available in the literature (see, e.g., Ref. 4), and will not be represented here.

The material property matrix, $\underset{\sim}{C}$ from Eq. (A-4), is expressed as

$$\underset{\sim}{C} = \begin{pmatrix} \underset{\sim}{C}_m & \underset{\sim}{0} \\ \underset{\sim}{0} & \underset{\sim}{C}_s \end{pmatrix} \quad , \tag{A-8}$$

where $\underset{\sim}{C}_m$ represents the in-plane material properties, and $\underset{\sim}{C}_s$ represents the material properties of the shear segments, where $\underset{\sim}{C}_s^{i,j}$ is expressed as

$$\underset{\sim}{C}^{i,j} = G^{i,j} \begin{bmatrix} 1 & 0 \\ 0 & 1 \end{bmatrix} ,$$

with $G^{i,j}$ denoting the interlaminar shear modulus.

The elastic stiffness matrix can now be separated into its membrane and interlaminar components by substituting Eqs. (A-7) and (A-8) into the first of Eqs. (A-6), resulting in

$$\underset{\sim}{k} = \underset{\sim}{k}_m + \underset{\sim}{k}_s ,$$

where

$$\underset{\sim}{k}_m = \int_V \underset{\sim}{W}_m' \, \underset{\sim}{C}_m \, \underset{\sim}{W}_m \, dV \quad , \quad \underset{\sim}{k}_s = \int_V \underset{\sim}{W}_s' \, \underset{\sim}{C}_s \, \underset{\sim}{W}_s \, dV$$

Written explicitly,

$$\underset{\sim}{k}_m = \begin{bmatrix} \underset{\sim}{k}_m^1 & & & \\ & \underset{\sim}{k}_m^2 & & \\ & & \ddots & \\ & & & \underset{\sim}{k}_m^n \end{bmatrix} , \quad \underset{\sim}{k}_s = \frac{A}{9} \begin{bmatrix} \underset{\sim}{p}^{1,2} & -\underset{\sim}{p}^{1,2} & & \\ -\underset{\sim}{p}^{1,2} & \underset{\sim}{p}^{1,2} + \underset{\sim}{p}^{2,3} & -\underset{\sim}{p}^{2,3} & \\ & -\underset{\sim}{p}^{2,3} & \ddots & \\ & & & \underset{\sim}{p}^{n-1,n} \end{bmatrix}$$

(A-9)

where A is the plane area of the element,

$$\underset{\sim}{p}^{i,j} = \frac{G^{i,j}}{t^{i,j}} \begin{bmatrix} 1 & 0 & 1 & 0 & 1 & 0 \\ 0 & 1 & 0 & 1 & 0 & 1 \\ 1 & 0 & 1 & 0 & 1 & 0 \\ 0 & 1 & 0 & 1 & 0 & 1 \\ 1 & 0 & 1 & 0 & 1 & 0 \\ 0 & 1 & 0 & 1 & 0 & 1 \end{bmatrix} ,$$

and $\underset{\sim}{k}_m^i$ is the stiffness matrix for the i^{th} orthotropic layer. The material properties and thickness can be varied from layer to layer, as can be seen from Eqs. (A-9).

Allowing plastic deformation in the interlaminar region only,

$$\underset{\sim}{\epsilon}_p = (\underset{\sim}{0} \quad \underset{\sim}{\gamma}^p) \quad .$$

This reduces $\underset{\sim}{k}_p \underset{\sim}{\epsilon}_o$ in Eq. (A-5) to $\underset{\sim}{k}_p^* \underset{\sim}{\gamma}_o^p$, where $\underset{\sim}{k}_p^{*i,j}$ is expressed as

$$\underset{\sim}{k}_p^{*i,j} = \frac{G^{i,j}A}{3} \begin{bmatrix} 1 & 0 & 1 & 0 & 1 & 0 & -1 & 0 & -1 & 0 & -1 & 0 \\ 0 & 1 & 0 & 1 & 0 & 1 & 0 & -1 & 0 & -1 & 0 & -1 \end{bmatrix}$$

APPENDIX B

NORMAL INTERLAMINAR SHEAR

A closed form solution for a $[0/90]_s$ laminate is obtainable by using the methods of Ref. 1 where, as mentioned in the text, the model is the same as that used in this paper. In the following, the notation used is that of Ref. 1. The reduced stiffness coefficients are

$$Q_{11}^{(1)} = Q_{22}^{(2)} = Q_{11}$$

$$Q_{22}^{(1)} = Q_{11}^{(2)} = Q_{22}$$

$$Q_{12}^{(1)} = Q_{12}^{(2)} = Q_{12}$$

$$Q_{33}^{(1)} = Q_{33}^{(2)} = Q_{33}$$

This leads to a set of differential equations as follows:

$$\begin{aligned} (Q_{33}\rho - k)A + kB &= 0 \\ (Q_{33}\rho - k)B + kA &= 0 \\ (Q_{22}\rho - k)C + kD &= 0 \\ (Q_{11}\rho - k)D + kC &= 0 \quad , \end{aligned} \tag{B-1}$$

where $k = G/hh_o$, and the coefficients correspond to the magnitudes of the displacements,

$$u_1 = Ae^{\rho y} \quad , \quad u_2 = Be^{\rho y} \quad , \quad V_1 = Ce^{\rho y} \quad , \quad V_2 = De^{\rho y}, \tag{B-2}$$

at the center, $y = 0$. The four roots of Eqs. (B-1), and their corresponding amplitude ratios are

$$\begin{aligned} \rho_1 &= 2k/Q_{33} & , \quad A_1 &= -B_1 \\ \rho_2 &= 0 & , \quad A_2 &= B_2 \\ \rho_3 &= k(Q_{11} + Q_{22})/Q_{11}Q_{22} & , \quad C_3 &= -(Q_{11}/Q_{22})D_3 \\ \rho_4 &= 0 & , \quad C_4 &= D_4 \quad . \end{aligned} \tag{B-3}$$

Substituting Eqs. (B-3) into the displacement representation, Eqs. (B-2), and using the stress-strain relations, we have

$$\tau_{zx} = (G/h)(u_1 - u_2) \quad , \quad \tau_{zy} = (G/h)(V_1 - V_2)$$

$$\begin{Bmatrix} \sigma_x^i \\ \sigma_y^i \\ \tau_{xy}^i \end{Bmatrix} = \begin{bmatrix} Q_{11}^{(i)} & Q_{12}^{(i)} & Q_{13}^{(i)} \\ & Q_{22}^{(i)} & Q_{23}^{(i)} \\ \text{SYMM} & & Q_{33}^{(i)} \end{bmatrix} \begin{Bmatrix} \epsilon_x^i \\ \epsilon_y^i \\ \gamma_{xy}^i \end{Bmatrix} , \qquad i = 1,2 \ ;$$

the laminate stresses are obtained,

$$\sigma_y^1 = -\sigma_y^2 = -\frac{u^*}{a} Q_{12} \frac{(Q_{22} - Q_{11})}{(Q_{11} + Q_{22})} \left(1 - \frac{\text{ch } \sqrt{\rho}\, y}{\text{ch } \sqrt{\rho}\, b}\right)$$

$$\sigma_x^1 = \frac{u^*}{a} \left[Q_{11} - \frac{2Q_{12}^2}{Q_{11} + Q_{22}} + \frac{Q_{12}^2 (Q_{22} - Q_{11})}{Q_{22}(Q_{11} + Q_{22})} \frac{\text{ch } \sqrt{\rho}\, y}{\text{ch } \sqrt{\rho}\, b} \right]$$

$$\sigma_x^2 = \frac{u^*}{a} \left[Q_{22} - \frac{2Q_{12}^2}{Q_{11} + Q_{22}} - \frac{Q_{12}^2 (Q_{22} - Q_{11})}{Q_{11}(Q_{11} + Q_{22})} \frac{\text{ch } \sqrt{\rho}\, y}{\text{ch } \sqrt{\rho}\, b} \right]$$

$$\tau_{zy} = \frac{u^*}{a} Q_{12} \frac{G(Q_{22} - Q_{11})}{hQ_{11}Q_{22}\sqrt{\rho}} \frac{\text{sh } \sqrt{\rho}\, y}{\text{ch } \sqrt{\rho}\, b} \quad ,$$

where

$$\rho = k(Q_{11} + Q_{22})/Q_{11}Q_{22}hh_o \quad .$$

For sufficiently wide plates the classical plate theory solution is recovered in the central region of the laminate.